Characterization of Surface-Charge-Mosaic-Modified Ultrafiltration Membranes Prepared by Laser-Induced Surface Graft Polymerization

NOBORU SAITO, SHUZO YAMASHITA

TERUMO Corporation R & D Center, 1500 Inokuchi, Nakai-machi, Ashigarakami-gun, Kanagawa 259-01, Japan

Received 19 November 1996; accepted 1 July 1997

ABSTRACT: Surface-charge-mosaic-modified ultrafiltration membranes with charged domains of various sizes (500, 100, or 50 μm) were prepared by two-step laser-induced surface graft polymerization using a striped photomask. First, the surface of an ultrafiltration membrane was treated with 4-vinylpyridine after laser irradiation using a striped photomask. Subsequently, the striped photomask was shifted and the surface that was initially shaded from the laser beam by the photomask was exposed to laser irradiation and treated with acrylic acid. The surface element distribution, surface chemical structure, and ion-exchange capacities of the treated membrane were determined by scanning X-ray photoelectron spectroscopy (XPS) analysis, time-of-flight secondary ion mass spectrometry (TOF-SIMS) with imaging capacities, and acid–base titration, respectively. Oxygen and carbon distribution maps determined by the scanning XPS analysis and the TOF-SIMS maps for $^{16}O^-$ and $^{26}CN^-$ ions show that the surface of the treated membrane had striped domains composed of poly(4-vinylpyridine) and poly(acrylic acid). The anion- and cation-exchange capacities of the treated membranes were approximately 2.0 mEq/m^2. The ultrafiltration rate of these membranes was markedly lower than that of a nontreated ultrafiltration membrane, but increased as the charge domain size decreased. The membrane flux of sodium ions also increased with decreasing charge domain size. This tendency was much stronger for sodium ions than for glucose. © 1998 John Wiley & Sons, Inc. J Appl Polym Sci **67:** 1141–1149, 1998

Key words: charge-mosaic-membranes; laser; surface graft polymerization; charge domain; selective transport

INTRODUCTION

Many studies have been conducted on selective transport membranes. In 1932, Söllner[1] proposed a charge-mosaic membrane consisting of anion- and cation-exchange regions. The phenomenological theory proposed by him is as follows: anions and cations can permeate through their respective countercharge regions in the membrane, resulting in current circulation between individual ion-exchange regions. As a result, the charge-mosaic membrane shows negative osmosis and much more efficient electrolyte transport than nonelectrolyte transport. The existence of circulating currents within a charge-mosaic membrane was predicted theoretically by Kedem and Katchalsky[2] and investigated experimentally by Weinstein et al.[3] More recently, Fujimoto and coworkers succeeded in fabricating a charge-mosaic membrane which shows selective transport behavior for ionized solutes.[4,5] This charge-mosaic membrane, which is commercially available as Desalton® (Tosoh Co., Ltd., Tokyo, Japan), has a microphase-

Correspondence to: Noboru Saito.

Journal of Applied Polymer Science, Vol. 67, 1141–1149 (1998)
 CCC 0021-8995/98/061141-09

separated structure (domain size ~ 50 nm) containing striped regions of positive and negative charges provided by a pentablock copolymer, poly[isoprene-*block*-styrene-*block*-butadiene-*block*-(4-vinylbenzyl)dimethylamine-*block*-isoprene]. Various techniques have been developed for preparing charge-mosaic membranes, such as involving the use of polymer blends[6–8] or latex[9] or epitaxial phase growth.[10] However, only a few attempts to obtain a charge-mosaic membrane by polymer grafting have been made. Chapiro et al. prepared a charge-mosaic membrane (domain size 500 μm) in a polytetrafluoroethylene (PTFE) substrate by X-ray-induced graft polymerization, with acrylic acid and 4-vinylpyridine, using a striped photomask made of brass (line-and-space width 500 μm).[11]

In recent years, a new type of membrane composed of a neutral porous substrate and a grafted polyelectrolyte filling the substrate pores has been proposed.[12,13] This new type of membrane combines the properties of a surface-modified microfiltration membrane with those of a highly charged ion-exchange membrane.

Previously we developed a laser-induced surface graft polymerization method in which surface radicals are generated by laser-irradiation-initiated radical polymerization.[14] This method enables surface graft polymerization with micron-order dimensional precision. We have extended the laser-induced graft polymerization method to the preparation of a surface-charge-mosaic-modified ultrafiltration membrane. The objective of this study is to develop an ultrafiltration membrane with a selective transport rate of ionic solutes as high as that of a charge-mosaic membrane. In this paper, we report on the preparation of surface-charge-mosaic-modified ultrafiltration membranes having charge domains of various sizes by two-step laser-induced surface graft polymerization using a striped photomask, and compare the permeability of the membranes to an ionic solute (NaCl) to that of a nonionic solute (glucose).

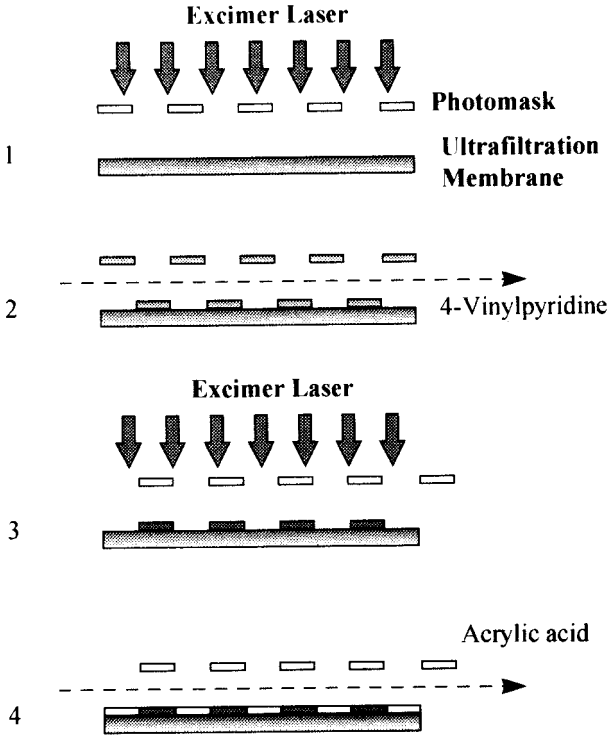

Figure 1 Schematic outline of the procedure for fabricating surface-charge-mosaic-modified ultrafiltration membrane. Surface graft polymerization was performed onto an ultrafiltration membrane with micro-order regional precision using the photomask.

EXPERIMENTAL

Materials

Ultrafiltration membranes (m.w. cut-off 20,000; diameter 25 mm), made of poly(*m*-phenylene isophthalamide), were purchased from Toyo Roshi Kaisha, Ltd. (Tokyo, Japan). Acrylic acid and 4-vinylpyridine, purchased from Tokyo Chemical Industry Co., Ltd. (Tokyo, Japan), were purified by distillation. Three types of striped photomask made of stainless steel and having line-and-space widths of 500, 100, and 50 μm, were designed for use in the preparation of the surface-charge-mosaic-modified ultrafiltration membranes and were fabricated at Nippon Filcon Co., Ltd. (Tokyo, Japan) by standard lithographic and etching techniques. A charge-mosaic membrane, Desalton®, prepared from a pentablock copolymer, was purchased from Tosoh Co., Ltd. (Tokyo, Japan).

Preparation of Surface-Charge-Mosaic-Modified Ultrafiltration Membranes by Laser-Induced Graft Polymerization

Laser-induced graft polymerization was carried out in a reaction chamber equipped with two valves, a Pirani gauge, and a quartz window (thickness: 5 mm). Details of the apparatus are given elsewhere.[14] Figure 1 outlines the two-step surface graft polymerization process using the striped photomask (line-and-space width: 500,

100, or 50 μm). First, an ultrafiltration membrane covered with a striped photomask was placed on the sample stage in the reaction chamber. Then, after the chamber was evacuated to 6.6 Pa, the membrane was irradiated through the quartz window at 10 mJ/cm^2 with 10 pulses, using a Hamamatsu Photonics Model L4500 excimer laser (Hamamatsu, Japan) at 248 nm KrF emission with a pulse width of 15 ns. After closing the valve on the vacuum line, the valve on the monomer-inlet line was opened to feed the 4-vinylpyridine vapor (vapor pressure: 2660 Pa) into the chamber. The monomer gas pressure was controlled by the valve on the monomer-inlet line. After 10 min, the valve on the monomer-inlet-line was closed and that on the vacuum line was opened to degas the chamber. Next, the photomask was shifted 500, 100, or 50 μm, according to the line-and-space width of the striped photomask used, by a micrometer linked to the photomask. Then, the membrane was irradiated at 10 mJ/cm^2 with 10 pulses *in vacuo.* By using the same method as in the first step, the acrylic acid vapor (1330 Pa) was fed into the chamber for 10 min. The treated membrane was thoroughly washed with methanol for removal of the nonreacted monomers and homopolymers, and then dried in air.

Imaging of Surface Chemical Structure and Morphology

The surface elemental distribution of graft-polymerized membranes was mapped by small-spot XPS[15] (Model SSX-100, Surface Science Instruments, USA) which has the capability of obtaining X-ray photoelectron spectra from areas as small as 0.15 mm at a take-off angle of 35°.

The surface chemistry of the graft-polymerized membranes was characterized by time-of-flight secondary ion mass spectrometry (TOF-SIMS)[16] with imaging capacities. All spectra and images were acquired using a PHI model TFS-2000 TOF-SIMS system (Charles Evans & Associates, CA, USA). The primary ion beam consisted of 25 KeV Ga^+ ions generated from a liquid metal field emission source. The pulse width of the primary ion source was 8.3 ns. The total ion dose was 8.1×10^{11} ions/cm^2 and the mass resolution was 610. In principle, TOF-SIMS can be used to resolve 0.1–0.2 μm.[17]

The morphology of cross sections of the membranes was analyzed by field emission scanning electron microscopy (FE-SEM) (Model S-8000, Hitachi, Tokyo, Japan).

Ion-Exchange Capacity

A membrane was conditioned by alternating treatments with a large excess of 0.05*N* HCl or 0.05*N* NaOH aqueous solution, and then washed with deionized water. For determination of the cation-exchange capacity, the membrane was converted to free acid form by treatment with 0.05*N* HCl followed by thorough washing with deionized water. The membrane was then placed in 5.00 mL of 0.05*N* NaOH aqueous solution for 30 min, and 4.00 mL of the solution was titrated with 0.05*N* HCl aqueous solution. Anion exchange capacity was determined by similar methods.

Zeta Potentials

The streaming potentials, induced by filtering of an electrolyte solution through the membrane, were measured by use of a streaming potential analyzer (Shimadzu ZP-10B, Kyoto, Japan). For electrolyte solutions, 0.01*N* KCl solutions whose pH was adjusted by addition of 0.05*N* HCl or 0.05*N* NaOH aqueous solution were used. The zeta potentials were calculated from the streaming potentials according to the Helmholtz–Smoluchowski equation.

Ultrafiltration Rate (UFR)

The UFR was measured in the pressure range of 0.34–0.81 kg/cm^2 using a stirred ultrafiltration cell (model UHP-25, Toyo Roshi Kaisha Ltd., Tokyo, Japan). The test solution, 5.5 m*M* NaCl aqueous solution, was agitated with a magnetic stirrer. The filtrate was collected into a measuring cup.

Permeability of the Membrane to Sodium Ions and Glucose

The permeability of the membrane to sodium ions and glucose was investigated by the piezodialysis method. The apparatus used is illustrated in Figure 2. A custom-designed cell consisting of two compartments (75 cm^3 each) divided by a membrane was used. The effective area of the membrane was 3.14 cm^2. Compartment I was filled with an aqueous solution (70 mL) of pH 7.0 containing NaCl and glucose at an initial concentration of 5.5 m*M* each. Compartment II was filled with deionized water (40 mL). The concentrations of sodium ions and glucose in compartment II were measured with an F-23 ion meter connected

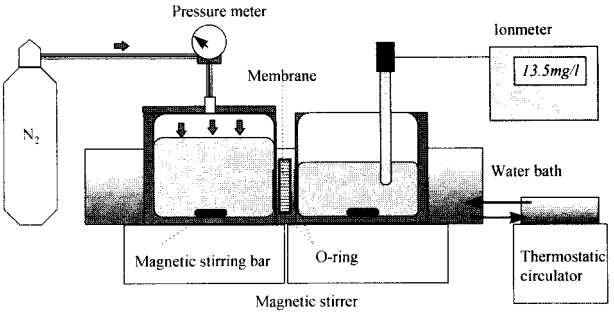

Figure 2 Schematic of the experimental apparatus for permeability measurements.

to a sodium ion-selective electrode (Horiba Ltd., Kyoto, Japan) and a blood glucose meter (ONE TOUCH II, Life Scan Inc., CA, USA), respectively. Both compartments were immersed in a water bath thermostated at 20°C and nitrogen gas was supplied to compartment I at a pressure of 0.34 kg/cm^2. Solute flux (J_s) was calculated from the slope of the initial straight line region of the concentration of solutes in compartment II versus time plots.

RESULTS

Preparation of Surface-Charge-Mosaic-Modified Ultrafiltration Membranes

As shown in Figure 1, the surfaces of ultrafiltration membranes were treated with 4-vinylpyridine by laser-induced surface graft polymerization using the striped photomask. Subsequently, with shifting of the photomask, the surface that was initially shaded from the laser beam by the photomask was exposed to laser irradiation and treated with acrylic acid. Elemental distribution maps of the surface of a membrane treated using the photomask (line-and-space width: 500 μm), determined by scanning XPS analysis, are shown in Figure 3. The oxygen distribution map (Fig. 3, right) shows high-concentration domains at $\sim$ 500 μm intervals, derived from acrylic acid. The carbon distribution map (Fig. 3, left) shows high-concentration domains at $\sim$ 500 μm intervals, derived from the difference in carbon content per monomer unit of 34% for acrylic acid and 47% for 4-vinylpyridine. Moreover, the graft-polymerized membranes were characterized by TOF-SIMS with imaging capacities. The negative TOF-SIMS spectra of the treated membranes showed the major peaks: m/z 16, 26, 42, and 43, which are assigned O^-, CN^-, CNO^-, and $C_2H_3O^-$, respectively (data not shown). The $^{16}O^-$ fragment ion is characteristic for poly(acrylic acid) and the $^{26}CN^-$ fragment ion is characteristic for poly(4-vinylpyridine). The fragment ions which were specific to the localized surface chemistry were used for imaging. For example, Figure 4 shows the TOF-SIMS maps for $^{16}O^-$ and $^{26}CN^-$, which were acquired from the membrane treated using the photomask (line-and-space width: 100 μm). The $^{16}O^-$ map (Fig. 4, top) shows the expected striped pattern in which the highlight lines are 100 μm wide and spaced 100 μm apart, replicating the pattern of the photomask used. The $^{26}CN^-$ map (Fig. 4, bottom) also clearly shows the striped pattern, which is complementary to the highlight lines for the $^{16}O^-$ map. These results clearly demonstrate the separation of the poly(acrylic acid) domain and the poly(4-vinylpyridine) domain corresponding to dimension of the used photomask.

The structure of cross sections of the membranes was analyzed by FE-SEM. In Figure 5, typical cross sections of a nontreated (Fig. 5, left) and a treated membrane (Fig. 5, right) are presented. Although the XPS spectra and TOF-SIMS spectra of the treated membranes were drastically different from those of the nontreated ones, no significant morphological change was detected even after the laser-induced graft polymerization. The treated membranes still appeared to have the typical asymmetric pore structure with a skin layer and finger-like cavities underneath, as shown in Figure 5. One may say that the laser-induced graft polymerization occurs to a limited extent on the surface of the membranes.

Ion-exchange capacities of treated membranes were determined by acid–base titration. The re-

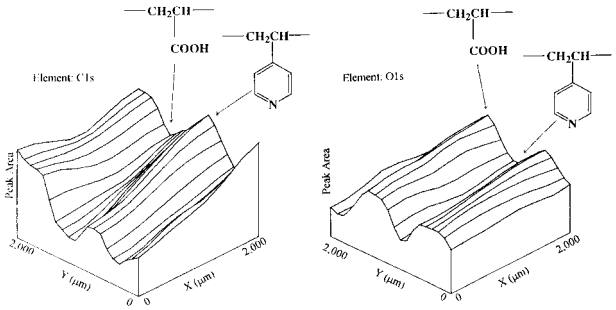

Figure 3 Elemental distribution maps (obtained by small-spot XPS) of a membrane treated using the photomask (line-and-space width: 500 μm). Right: oxygen (Ols) distribution map; left: carbon (C1s) distribution map.

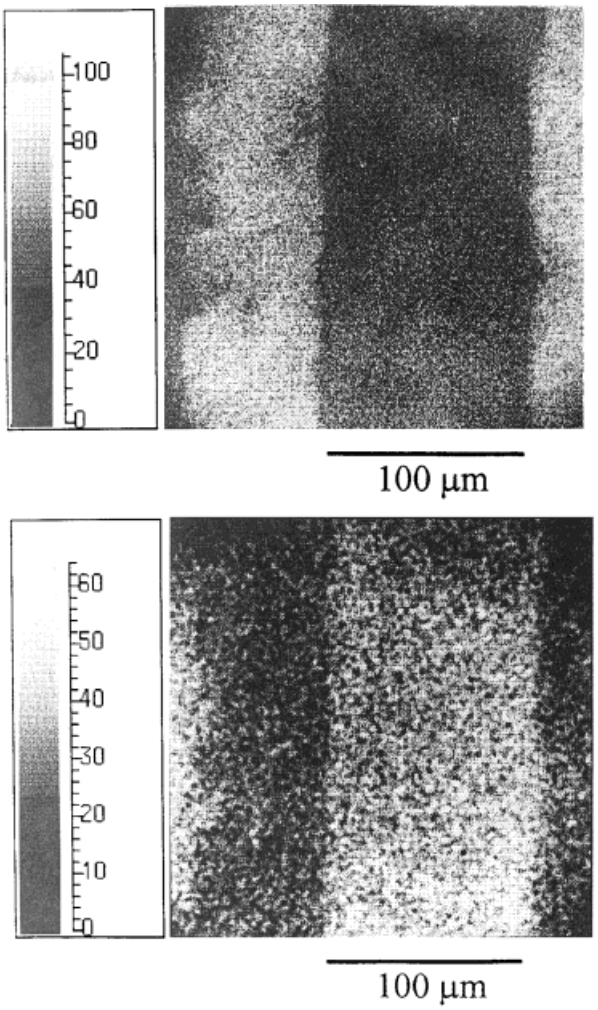

Figure 4 TOF-SIMS maps for $^{16}O^-$ and $^{26}CN^-$ of a membrane treated using the photomask (line-and-space width: 100 μm). The light areas correspond to regions where counts were detected. Top: location of the $^{16}O^-$ fragment derived from poly(acrylic acid); bottom: location of the $^{26}CN^-$ fragment derived from poly(4-vinylpyridine).

sults corresponding to the line-and-space width of the striped photomask used are as follows: the cation-exchange capacities were 2.0 mEq/m^2 for 500 μm, 2.5 mEq/m^2 for 100 μm, and 3.2 mEq/m^2 for 50 μm; and the anion-exchange capacities were 2.2 mEq/m^2 for 500 μm, 2.0 mEq/m^2 for 100 μm, and 2.2 mEq/m^2 for 50 μm.

The results confirm that membranes treated by laser-induced surface graft polymerization were surface - charge - mosaic - modified ultrafiltration membranes containing alternating striped domains of positive and negative charges. These membranes were coded according to the domain size as M500, M100, and M50.

Zeta Potentials

The zeta potentials calculated from the streaming potentials are shown in Figures 6 and 7. The zeta potentials of the poly(acrylic acid)-grafted membrane had negative values irrespective of pH, indicating cation-exchange membrane properties, independent of pH. The zeta potential of the poly(4-vinylpyridine)-grafted membrane was dependent on pH. It is clear that the poly(4-vinylpyridine)-grafted membrane is in a protonated state and played the role of an anion-exchange membrane at low pH (<4). On the other hand, the zeta potentials of the surface-charge-mosaic-modified ultrafiltration membranes were ~ 0 mV irrespective of domain size. Hence the zeta potentials of these membranes were negligibly dependent on pH.

Ultrafiltration Rate (UFR)

Figure 8 shows the relationship between the UFR of the surface-charge-mosaic-modified ultrafiltration membranes and the transmembrane pressure (TMP). The UFR of the membranes increased linearly with increasing TMP. The filtration coefficient (L_p) depended on the charge domain size of the membranes: 0.007 mL min^{-1} kg^{-1} for M500; 0.009 mL min^{-1} kg^{-1} for M100, and 0.019 mL min^{-1} kg^{-1} for M50. These values increased with decreasing charge domain size of the membranes; however, these values were still lower than that of the nontreated membrane (0.126 mL min^{-1} kg^{-1}).

Permeability of the Membrane to Sodium Ion and Glucose on Piezodialysis

Figure 9 shows the results of piezodialysis, plotted as the concentrations of sodium ions (Na^+) and glucose in compartment II versus piezodialysis time. Solute fluxes (J_s), calculated from the initial slopes of the curves, are summarized in Table I. The flux of sodium ions (J_{Na}) through the membranes increased markedly with decreasing charge domain size, whereas that of glucose ($J_{glucose}$) increased slightly with decreasing charge domain size. The permeation selectivity coefficient ($J_{Na}/J_{glucose}$) indicated increased selective permeation for sodium ions with decreasing charge domain size of the membranes: 1.5 for M500, 6.0 for M100, and 6.7 for M50. However, these values were markedly different from that of 45.3 for the charge-mosaic membrane, Desalton®.

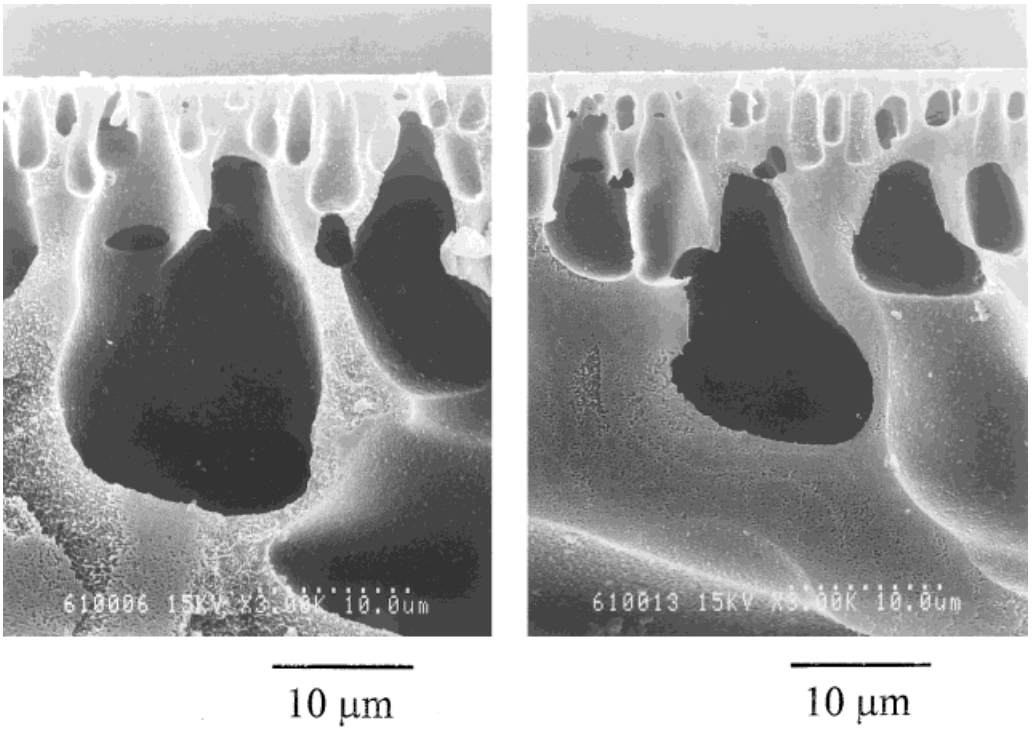

Figure 5 Field emission scanning electron micrographs (FE-SEM) of a cross section of a nontreated membrane and a treated membrane. Left: nontreated membrane (×3000); right: membrane treated using the photomask (line-and-space width: 100 μm) (×3000).

DISCUSSION

Two-step laser-induced surface graft polymerization with a photomask was used to prepare surface-charge-mosaic-modified ultrafiltration membranes, whose surfaces were graft-polymerized alternately with poly(acrylic acid) and poly(4-vi-

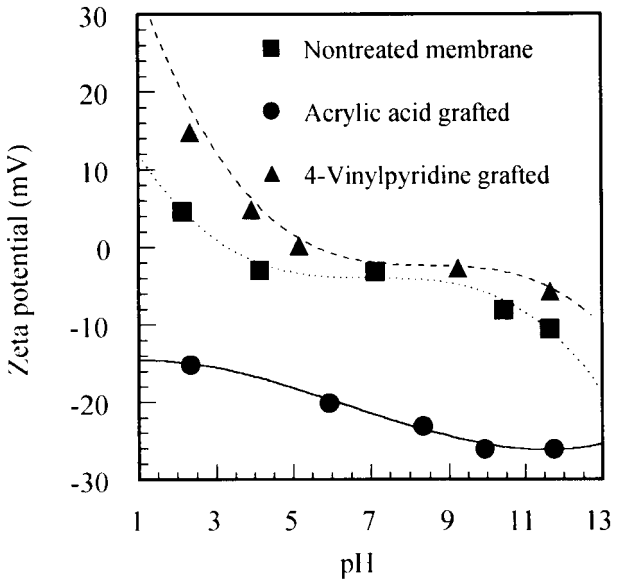

Figure 6 Dependence of zeta potentials of membranes on pH. (■) nontreated; (●) treated with acrylic acid; (▲) treated with 4-vinylpyridine.

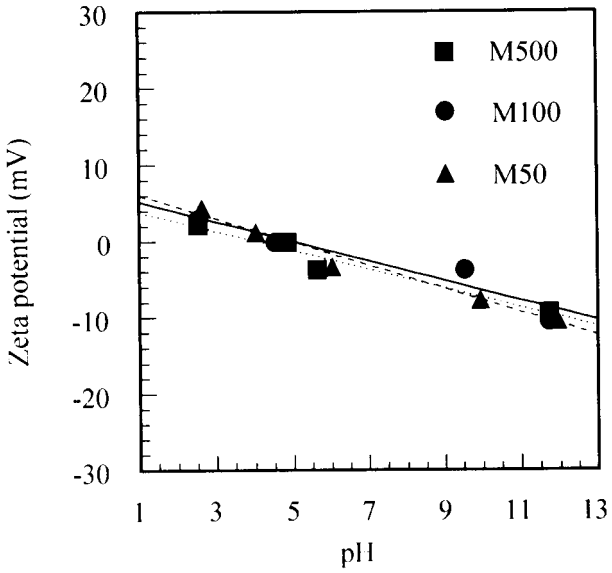

Figure 7 Dependence of zeta potentials of the surface-charge-mosaic-modified ultrafiltration membranes on pH. (■) M500; (●) M100; (▲) M50.

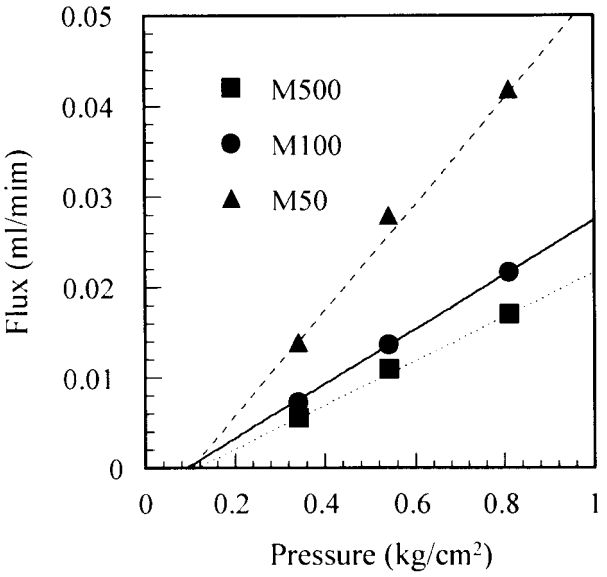

Figure 8 Relationship between ultrafiltration rate and transmembrane pressure for the surface-charge-mosaic-modified ultrafiltration membranes. (■) M500; (●) M100; (▲) M50.

nylpyridine) in parallel. There is strong evidence that the surfaces of these membranes contain alternating striped domains of poly(acrylic acid) and poly(4-vinylpyridine). Surface elemental distribution maps (Fig. 3), determined by scanning XPS analysis, show that there is a high concentration domain of oxygen derived from poly(acrylic acid) and carbon derived from poly(4-vinylpyridine), corresponding to the pattern dimensions of the photomask used. Furthermore, surface mass spectral information obtained by TOF-SIMS with imaging capacities was useful for determining the surface chemical structure of the membranes. The TOF-SIMS maps for $^{16}O^-$ and $^{26}CN^-$ ions (Fig. 4), specific to the localized surface chemistry, show the expected striped pattern replicating the pattern of the photomask used. These results clearly demonstrate that the surfaces of these membranes contain alternating striped domains of poly(acrylic acid) and poly(4-vinylpyridine) corresponding to the pattern dimensions of the photomask used. The UFR of these membranes was markedly lower than that of a nontreated ultrafiltration membrane, which suggests that pores in the treated ultrafiltration membranes are covered with grafted polymers, based on the limited occurrence of laser-induced graft polymerization on the surface of the membranes as described in the results section for the membrane morphology. Therefore, it appears that the surface-charge-mosaic-modified ultrafiltration membranes are composed of a porous substrate and a mosaic-grafted polyelectrolyte which covers the substrate pores. As shown in Figure 8, the UFR of the membranes increased with decreasing charge domain size of the membrane. Upon piezodialysis, the flux of sodium ions through the membranes increased with decreasing charge domain size and was much greater than that of glucose. The permeation selectivity coefficient of the membranes, $J_{Na}/J_{glucose}$, indicated increasingly selective permeation of sodium ions with decreasing charge domain size of the membranes (Table I). As mentioned above, these surface-charge-mosaic-modified ultrafiltration membranes have properties similar to those of a charge-mosaic membrane.

Therefore, these properties may be explained in terms of a battery model of a charge-mosaic membrane consisting of alternating anion- and cation-exchange membranes arranged in parallel, as proposed by Weinstein, Bunow, and Caplan et al.[18] and shown in Figure 10. According to their theory, applying pressure (ΔP) to one side of the ion-exchange membrane immersed in an aqueous salt solution induces a streaming potential ($\Delta\Phi$)

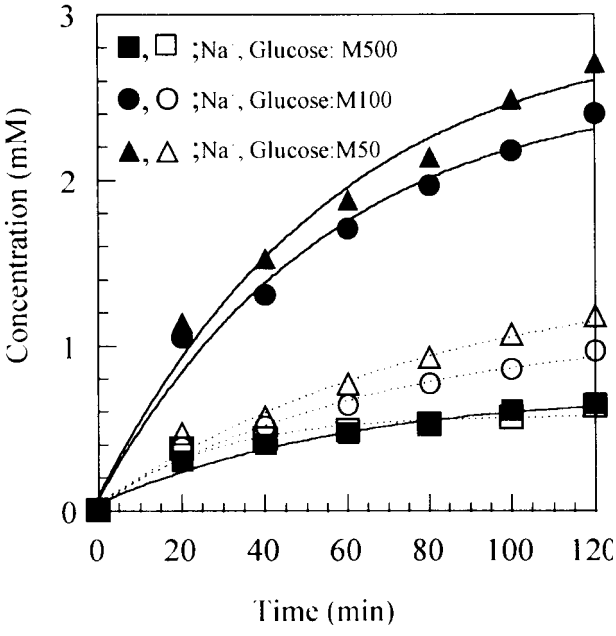

Figure 9 Time course of concentrations of sodium ions and glucose in compartment II for the surface-charge-mosaic-modified ultrafiltration membranes. M500 [(●) Na^+; (○) glucose]; M100 [(■) Na^+; (□) glucose]; M50 [(▲) Na^+; (△) glucose].

Table I Solute Flux, J_S, of the Surface-Charge-Mosaic-Modified Ultrafiltration Membranes and Commercial Charge-Mosaic Membrane (Desalton®) in Piezodialysis Mode

Membrane	Domain Size (μm)	$J_{Na} \times 10^8$ (mol^{-1} l^{-1} cm^{-2} s^{-1})	$J_{glucose} \times 10^8$ (mol^{-1} l^{-1} cm^{-2} s^{-1})	$J_{Na}/J_{glucose}$
M500	500	2.0	1.3	1.5
M100	100	19.9	3.3	6.0
M50	50	25.3	3.7	6.7
Desalton	0.05	40.8	0.9	45.3

Pressure = 0.34 kg cm^{-2}.

proportional to the pressure, which is expressed as

$$\Delta\Phi = -\beta'\Delta P, \qquad (1)$$

where β' is the electro-osmotic coefficient, which is positive for cation-exchange membranes and negative for anion-exchange membranes. Therefore, on anion- and cation-exchange domains in a charge-mosaic membrane, the directions of electric current induced by the streaming potential oppose each other, producing a loop current. The loop current facilitates transport of ionic solutes. As a result, the charge-mosaic membrane enables effective permeation of ionic solutes from mixtures of ionic and nonionic solutes. The loop conductance of the electric current for the membrane, κ'_{loop} is expressed as

$$\kappa'_{loop} = 1/(\gamma_a R_a + \gamma_c R_c + R_i + R_{ii}). \qquad (2)$$

Here, γ is the domain size, R is the electrical resistance, the a and c subscripts denote the anion- and cation-exchange regions, respectively, and the i and ii subscripts denote compartments I and II, respectively. According to eq. (2), κ'_{loop} increases with decreasing γ_a and γ_c; consequently, the flux of ionic solutes increases which induces an increase in the UFR since the ionic solute flux is accompanied by flux of water molecules bound to ionic solutes.[8] There is evidence that the properties of the surface-charge-mosaic-modified ultrafiltration membranes can be explained in terms of a battery model. In Figure 7, the zeta potentials of the surface-charge-mosaic-modified ultrafiltration membranes, calculated from the streaming potentials, were $\sim$ 0 mV independent of pH and charge domain size. This result can be explained quite naturally, as shown in Figure 10, by consumption of the streaming potentials in the loop current. Here, it may be necessary to explain that the absence of insulation separating opposite charge domains is not important. An anion cation-exchange junction offers highly effective resistance to direct current flow of either polarity.[10,11] Figure 11 shows the relationship between the flux of sodium ions (J_{Na}) and the charge domain size. The relationship can be expressed by a reciprocal function, which is in agreement with the relationship between the loop conductance of electric current, κ'_{loop}, and the charge domain size of the charge-mosaic membranes, γ_a, and γ_c, as expressed by eq. (2).

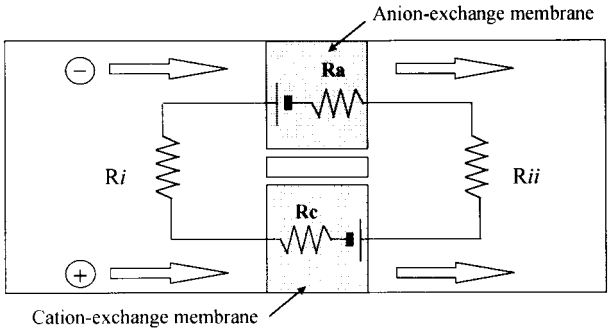

Figure 10 Battery model of charge-mosaic membrane, as proposed by Weinstein et al.[18] γ is domain size, R is electrical resistance, the a and c subscripts denote anion- and cation-exchange regions, respectively, and the i and ii subscripts denote compartments I and II, respectively.

J_{Na} increased markedly with decreasing charge domain size, and $J_{Na}/J_{glucose}$ indicated increased selective permeation for sodium ions with decreasing charge domain size of the membranes: 1.5 for M500, 6.0 for M100, and 6.7 for M50. However, these values are markedly different from those of 45.3 for the charge-mosaic membrane, Desalton®. Several reasons are given to explain the difference. First, the charge domain size [γ in eq. (2)] is of micrometer order for M500, M100,

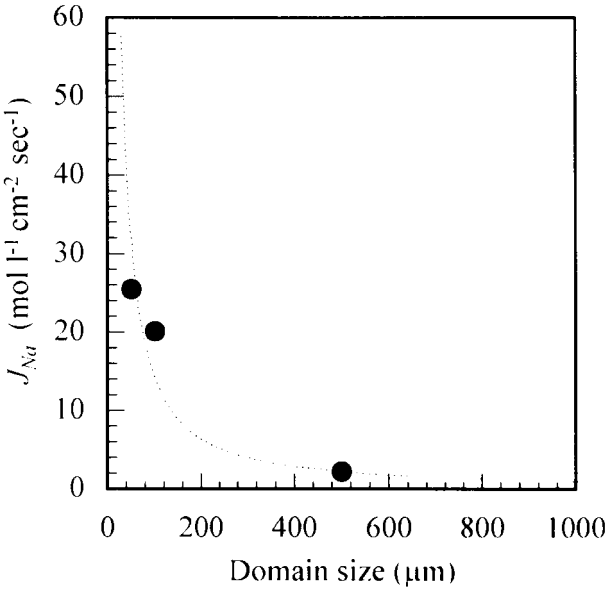

Figure 11 Relationship between flux of sodium ions and charge domain size of the surface-charge-mosaic-modified ultrafiltration membranes.

and M50; and nanometer order for Desalton®. Second, the electrolyte strength of the charge domains [corresponding to electrical resistance, R, in eq. (2)], is a weak polyelectrolyte for M500, M100, and M50 [poly(acrylic acid) and poly(4-vinylpyridine)], and a strong polyelectrolyte for Desalton® [sulfonated-poly(styrene) and poly(4-vinylpyridinium iodide)]. Third, the charge domain region, depending on the diffusion coefficient of organic solutes such as glucose,[18,19] is noncrosslinked for M500, M100, and M50, and physically crosslinked for Desalton®.[20]

We conclude that a surface-charge-mosaic-modified ultrafiltration membrane can be prepared by two-step laser-induced surface graft polymerization using a striped photomask. This process yields a new type of membrane with the combined properties of an ultrafiltration membrane and a charge-mosaic membrane. Further studies are required for determination of the permeability of the membranes to various ionic and nonionic solutes and development of a technique enabling surface graft polymerization with submicron-order dimensional precision.

The authors thank Dr. T. Matsuda and Dr. H. Nakayama, National Cardiovascular Center Research Institute (Osaka, Japan), for the use of the excimer-laser system in their laboratory. The small-spot X-ray photoelectron spectra and the TOF-SIMS spectra were measured at Toray Research Center, Inc. (Tokyo, Japan). This study was conducted under a research program (New Biomedical Foundation) fully supported by the Ministry of Welfare and Health, Japan.

REFERENCES

1. K. Söllner, *Biochem. Z.,* **244,** 370 (1932).
2. O. Kedem and A. Katchalsky, *Trans. Faraday Soc.,* **59,** 1931 (1963).
3. J. N. Weinstein, B. W. Misra, D. Kalif, and S. Caplan, *Desalination,* **12,** 1 (1973).
4. Y. Matsushita, H. Choshi, T. Fujimoto, and M. Nagasawa, *Macromolecules,* **13,** 1053 (1980).
5. T. Fujimoto and K. Ohkoshi, *J. Membrane Sci.,* **20,** 313 (1984).
6. R. Gajek and W. Trochimczuk, *J. Polym. Sci., Poly. Phys. Ed.,* **19,** 1663 (1981).
7. H. Kawatoh, M. Kakimoto, A. Tanioka, and T. Inoue, *Macromolecules,* **21,** 625 (1988).
8. K. L. Platt and A. Schindler, *Angew. Makromol. Chem.,* **19,** 135 (1971).
9. T. Eguchi and M. Shimokawa, *Jpn. Pat.* No. 53-18482 (1978).
10. K. Ishizu and M. Amemiya, *J. Membrane Sci.,* **65,** 129 (1992).
11. A. Chapiro, A. M. Jenderychowska-Bonamour, and S. Mizrahi, *Europ. Polym. J.,* **12,** 773 (1976).
12. T. Yamaguchi, S. Nakano, and S. Kimura, *Macromolecules,* **24,** 5522 (1991).
13. A. M. Mika, R. F. Childs, J. M. Dickson, B. E. McCarry, and D. R. Gagnon, *J. Membrane Sci.,* **108,** 37 (1995).
14. N. Saito, S. Yamashita, and T. Matsuda, *J. Polymer Sci. A: Polym. Chem.,* **35,** 747 (1997).
15. M. P. Seah and G. C. Smith, *Surf. Interface Anal.,* **11,** 69 (1988).
16. E. Niehuis, P. N. T. van Velzen, J. Lub, T. Heller, and A. Benninghorven, *Surf. Interface Anal.,* **14,** 135 (1989).
17. J. C. Vickerman, A. Brown, and N. M. Reed, *Secondary Ion Mass Spectrometry: Principles and Applications;* Clarendon, Oxford, UK (1989).
18. J. N. Weinstein, B. J. Bunow, and S. R. Caplan, *Desalination,* **11,** 341 (1972).
19. K. Ishizu and M. Iwade, *J. Appl. Polym. Sci.,* **52,** 1 (1994).
20. Y. Isono, H. Tanisugi, K. Endo, T. Fijimoto, H. Hasegawa, T. Hashimoto, and H. Kawai, *Macromolecules,* **16,** 5 (1983).